Cholesterol sulfate fluidizes the sterol fraction of the stratum corneum lipid phase and increases its permeability
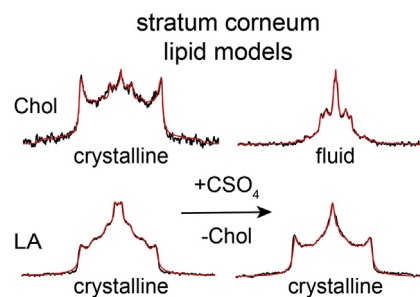
Ferdinand Fandrei[1], Oskar Engberg[1] , Lukáš Opálka[2] , Pavla Jančálková[2] , Petra Pullmannová[2] , Miloš Steinhart[3], Andrej Kováčik[2] , Kateřina Vávrová[2] , and Daniel Huster[1]*

[1]Institute of Medical Physics and Biophysics, University of Leipzig, Leipzig, Germany; [2]Skin Barrier Research Group, Faculty of Pharmacy, Charles University, Hradec Králové, Czech Republic; and [3]Institute of Macromolecular Chemistry, Czech Academy of Science in Prague, Prague, Czech Republic

Abstract Desulfation of cholesterol sulfate (CholS) to cholesterol (Chol) is an important event in epidermal homeostasis and necessary for stratum corneum (SC) barrier function. The CholS/Chol ratio decreases during SC maturation but remains high in pathological conditions, such as X-linked ichthyosis, characterized by dry and scaly skin. The aim of this study was to characterize the influence of the CholS/Chol molar ratio on the structure, dynamics, and permeability of SC lipid model mixtures. We synthesized deuterated CholS and investigated lipid models with specifically deuterated components using ^2H solid-state NMR spectroscopy at temperatures from 25°C to 80°C. Although the rigid acyl chains in ceramides and fatty acids remained essentially rigid upon variation of the CholS/Chol ratio, both sterols were increasingly fluidized in lipid models containing higher CholS concentrations. We also show the X-ray repeat distance of the lipid lamellar phase (105 Å) and the orthorhombic chain packing of the ceramide's acyl chains and long free fatty acids did not change upon the variation of the CholS content. However, the Chol phase separation visible in models with high Chol concentration disappeared at the 50:50 CholS/Chol ratio. This increased fluidity resulted in higher permeabilities to model markers of these SC models. These results reveal that a high CholS/Chol ratio fluidizes the sterol fraction and increases the permeability of the SC lipid phase while maintaining the lamellar lipid arrangement with an asymmetric sterol distribution.

Human skin protects the body from its surroundings and excessive water loss. Its main permeability barrier function is maintained by the stratum corneum (SC), which consists of corneocytes embedded in a multilamellar lipid matrix (1, 2). The three major SC lipid classes include ceramides (Cers), free fatty acids (FFAs), and cholesterol (Chol) in an approximately equimolar ratio (3), which is essential for a functional barrier (2–4). Cholesterol sulfate (CholS) as the most abundant Chol ester likely plays a special role in this matrix. Besides its effect as a regulator for epidermal differentiation (5), CholS is also desulfated by steroid sulfatase to Chol, one of the key barrier lipids. CholS concentration follows a gradient within human skin with a maximum of 5 wt% of the total lipids in the stratum granulosum declining to about 1 wt% in the outer SC (5). In X-linked ichthyosis (XLI) patients who lack steroid sulfatase, 3- to 5-fold higher CholS concentrations were measured at the expense of Chol concentration, leading to a CholS/ Chol ratio of approximately 1 (6, 7).

CholS is also interesting from chemical and biophysical points of view. In contrast to the predominantly nonpolar and hydrophobic lipid matrix, the highly polar and acidic sulfate group of CholS with a pK_a value of 3.3 (8) exhibits unique electrostatic properties and hydrogen bonding capacity, likely affecting the general organization of the lipid matrix. Biophysical and computer modeling studies on SC models have in detail analyzed the 3D structure of the SC lipid layer (9–12). In contrast to phospholipid membranes, which are highly hydrated and characterized by a high degree of molecular dynamics (13, 14), SC lipid layers are found to be very rigid and only contain one to two water molecules per lipid (9–12, 15). Introducing CholS with a

stratum corneum lipid models

*For correspondence: Daniel Huster, daniel.huster@medizin.uni-leipzig.de.

bulky polar headgroup could potentially loosen lipid packing by introducing packing defects and increase lipid hydration because of repulsive electrostatic forces between opposing lipid layers (16). As lipid packing is also closely related to the permeability of lipid layers (17), this important property could be influenced by CholS. Previous studies of skin lipid models showed that CholS diminished the phase-separated crystalline Chol and induced a fluid phase, displaced the association of FFAs with Ca^{2+} ions, and modulated the membrane polymorphism (18–20). A shift in pH-induced leakage was also described in vesicles composed of palmitic acid with Chol and/or CholS (21).

To better understand the effects of the altered CholS/Chol ratios in skin barrier lipids, we studied the influence of varying sterol compositions on the organization of the SC lipid model mixtures using ^{2}H NMR spectroscopy, X-ray diffraction, and permeability measurements. We compared three lipid model mixtures comprising the major SC lipid classes, only differing in their CholS/Chol ratios. In a simplified skin model without any CholS ("no CholS model," nCholS), an equimolar mixture of N-lignoceroyl-D-erythro-sphingosine (Cer[NS]), an FFA mix (22), and Chol was used as the reference sample. In a skin model with low CholS concentration ("low CholS model," lCholS) representing the CholS concentration in the healthy skin lipid barrier, the sterol phase was formed by 85 mol% Chol and 15 mol% CholS (i.e., the total CholS concentration was 5 mol% relative to all lipids). As elevated levels of CholS are reported for pathological skin conditions (23), a model with high CholS concentration was used containing Chol and CholS in an equimolar ratio ("high CholS model," hCholS), which corresponds to a total CholS content of 16.7 mol% of all lipids. The structures of the deuterated lipids used in ^{2}H NMR analysis are shown in **Fig. 1**.

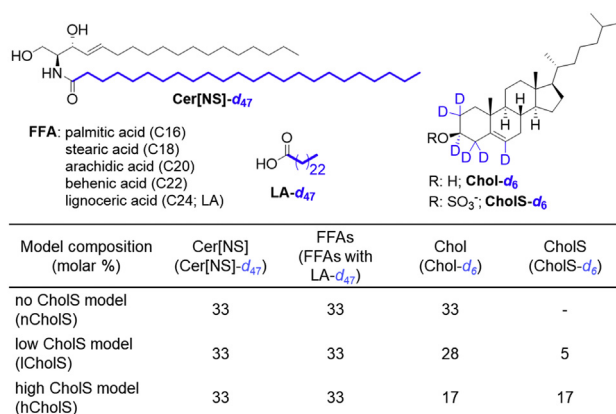These three model mixtures allowed us to systematically investigate the influence of CholS on the structure and dynamics of the SC lipid phase. It was observed that CholS mainly affects the sterol components of the lipid mix, although having only a minor influence on the organization of Cer and FFA acyl chains. From these results, we propose that a higher CholS/Chol proportion introduces higher fluidity. Our model confirms the previously proposed asymmetric sterol distribution within the lipid matrix of the SC based on X-ray diffraction techniques (24) but highlights the fluidizing effect of increasing CholS concentrations on the sterol components. This higher sterol fluidity is accompanied by an increase in the permeability of these lipid layers as observed in Franz cell diffusion experiments using four permeation markers. Thus, CholS induces rather significant modifications in the structure and dynamics of the SC lipid phase, which may be important for the early phases of the SC lipid assembly but later in the mature SC may lead to marked alterations of the integrity of the skin barrier.

MATERIALS AND METHODS

Materials

Chol, CholS, and Cer[NS] were purchased from Avanti Polar Lipids (Alabaster, AL). Deuterated Chol (^{2}H-2,2,3,4,4,6) (Chol-d_6) was purchased from Cambridge Isotope Laboratories, Inc (Tewksbury, MA), and perdeuterated lignoceric acid-d_{47} (LA-d_{47}) was purchased from Cayman Chemical (Ann Arbor, MI). The synthesis of deuterated N-lignoceroyl-D-erythro-sphingosine-d_{47} (Cer[NS]-d_{47}) was a one-step reaction of the sphingosine with LA as previously described (25). Palmitic acid, stearic acid, arachidic acid, behenic acid, and LA (all analytical or HPLC grade) were purchased from Sigma-Aldrich Chemie GmbH (Schnelldorf, Germany).

Synthesis of sodium cholesteryl sulfate-2,2,3,4,4,6-d_6

A volume of 75 µl (131 mg; 1.128 mmol) of HSO$_3$Cl was slowly added to 2 ml of dry pyridine at 0°C under an argon atmosphere, and the resulting milky suspension was stirred for 45 min. Subsequently, 37 mg (0.094 mmol) of Chol-d_6 in 3 ml of dry pyridine was added, temperature was increased to room temperature, and the reaction mixture was stirred under an argon atmosphere overnight. The reaction was terminated by addition of toluene and evaporation. Toluene was added and evaporated multiple times to remove all residues of pyridine. The crude product was dissolved in methanol, alkalized with a saturated solution of NaOH in methanol to a pH around 8, and evaporated with silica. The crude product was purified using column chromatography on silica with mobile phase toluene/ethanol 9:5 to 1:1 to yield 37 mg (79%) of a white solid. ^{1}H NMR (500 MHz, CD$_3$OD) δ 2.06 (dt, J = 12.7, 3.5 Hz, 1H), 1.98 (dd, J = 17.1, 4.8 Hz, ^{1}H), 1.89 (d, J = 13.5 Hz, 1H), 1.94–1.82 overlap (m, 1H), 1.71–1.24 (m, 10H), 1.25–1.07 (m, 6H), 1.07–0.99 (m, 4H), 0.99–0.93 (m, 3H), 0.89 (dd, J = 6.6, 1.9 Hz, 6H), 0.73 (s, 3H). ^{13}C NMR (126 MHz, CD$_3$OD) δ 141.39, 128.33, 58.13, 57.55, 51.63, 43.50, 41.13, 40.69, 38.26, 37.55, 37.37, 37.13, 33.20, 32.90, 30.78, 29.33, 29.16, 25.31, 24.94, 23.20, 22.95, 22.16, 19.74, 19.25, 12.32.

Fig. 1. Structures of the deuterated lipids used in this study. Deuterium labeling is indicated in blue.

Model composition (molar %)	Cer[NS] (Cer[NS]-d_{47})	FFAs (FFAs with LA-d_{47})	Chol (Chol-d_6)	CholS (CholS-d_6)
no CholS model (nCholS)	33	33	33	-
low CholS model (lCholS)	33	33	28	5
high CholS model (hCholS)	33	33	17	17

Sample preparation for ^{2}H NMR and X-ray diffraction

The lipid mixture for the model systems was constituted from an equimolar mixture of Cer[NS], FFAs, and Chol/CholS. For the FFA mixture, we used a mix of saturated FFAs at a molar ratio of C16:0 (1.8%), C18:0 (3.9%), C20:0 (7.5%), C22:0 (47.8%), and C24:0 (39.0%) similarly as described before (22). This mixture of saturated FFAs is highly relevant as the skin effectively sorts lipids so that the final SC mix is almost exclusively saturated (the content of unsaturated FFAs is approximately 2–3% (26)). We compared three lipid models with varying CholS content. In a simplified lipid mix (nCholS), the sample only contained Chol and no CholS. In two other skin models, the ratio of Chol and CholS was low (0.85:0.15, lCholS) or high (1:1, hCholS).

Each investigated lipid sample always contained one single deuterated lipid species, that is, either Cer[NS]-d_{47}, LA-d_{47}, Chol-d_6, or cholesterol sulfate-d_6 (CholS-d_6). Thus, structural and dynamic parameters for each deuterated component of the mixture could be obtained individually. For sample preparation, lipids were dissolved in chloroform/methanol (2:1) and mixed at their respective molar ratio. Afterwards, the solvent was evaporated using a rotary evaporator and redissolved in cyclohexane before lyophilization at ~0.1 mbar overnight, resulting in a fluffy powder. The lipid powder was then hydrated with 50 wt% aqueous buffer prepared with deuterium-depleted water at pH 5.4 (100 mM 2-(N-morpholino) ethanesulfonic acid, 100 mM NaCl, and 5 mM EDTA). After 10 freeze-thaw cycles (freezing of the sample in liquid nitrogen, heating to 80°C in a water bath), the samples were filled into 4 mm magic-angle spinning rotors and equilibrated at room temperature for a minimum of 24 h. To prevent dehydration of the ^{2}H NMR samples, the NMR rotors were sealed with an airtight cap.

Sample preparation for zeta potential measurement

The lipid mixtures were prepared similarly as the ^{2}H NMR samples. For hydration, same skin buffer as described before (pH 5.4) was used to dilute sample to 1 mM. After 10 freeze-thaw cycles, samples were sonicated for 15 min using a tip sonifier.

Sample preparation for permeability experiments

The three model systems (nCholS, lCholS, and hCholS) were prepared as described above, but only contained protiated lipids. The lipids were dissolved in chloroform/methanol (2:1), evaporated under a stream of nitrogen, and vacuum dried over P_2O_5 and solid paraffin for 24 h. Nuclepore track-etched polycarbonate filters of 0.015 mm pore size (Whatman, Kent, Maidstone, UK) were washed in 2:1 hexane/96% ethanol (v/v), dried, and mounted in steel holders. The lipids were redissolved in the hexane/ethanol mix at 4.5 mg/ml and sprayed on the filters (2 × 100 μl/cm^2) under a stream of nitrogen using a Linomat 5 (Camag, Muttenz, Switzerland) equipped with an additional module for y-axis movement. The lipid films were hydrated at 80°C with MES buffer at pH 5.4 for 10 min and slowly (over 4 h) cooled down to a temperature of 32°C.

^{2}H NMR spectroscopy

Stationary ^{2}H NMR measurements were acquired on a Bruker Avance I 750 NMR spectrometer (Bruker BioSpin, Rheinstetten, Germany) at a resonance frequency of 115.15 MHz for ^{2}H using a solid probe with a 5 mm solenoid coil. A spectral width of ±250 kHz was applied using quadrature phase detection, a phase cycled quadrupolar echo sequence (27) with two 2.5–3.5 μs 90° pulses separated by a 30 μs delay. The recycle delay was 50 s for samples that featured orthorhombic phase portions to account for proper relaxation (28). Samples were measured at temperatures of 25, 32, 50, 65, and 80°C and processed using a program written in Mathcad (MathSoft, Cambridge, MA) (29). Typically, one ^{2}H NMR spectrum was accumulated per sample; selected samples were remeasured to confirm reproducibility.

^{2}H NMR line shape simulations

^{2}H NMR line shapes were simulated assuming a superposition of ^{2}H NMR Pake doublets with a quadrupolar coupling constant of 167 kHz, scaled by the adequate order parameter (S) and normally one isotropic line as described previously (30). The relative proportions of each individual phase observed in the ^{2}H NMR spectra were directly determined from these fits. Quantification of these ^{2}H NMR spectra was possible because of the long delay times between successive scans (approximately 5 × T_1, T_1 ~ 10 s) (28, 30, 31). The relative contributions of the different phases were determined from the relative area under the curve for each individual line shape of each phase that contributed to the final NMR spectrum of the respective sample.

X-ray scattering measurements

Samples were characterized by small-angle X-ray scattering (SAXS) and near wide-angle X-ray scattering (NWAXS) at room temperature. Measurements were performed by means of the point focusing SAXS instrument (originally Molecular Metrology, recently considerably upgraded by SAXSLAB, now Xenocs). The CuKα beam with the wavelength of λ = 0.154 nm was generated by Rigaku Micromax-003, which is a low-power microsource equipped with X-ray optics working at $U = 50$ kV and $I = 0.6$ mA. Scattering was detected by the 2D detector Pilatus3 300K (Dectris) at two different distances of 0.541 and 0.052 m from the sample. After merging data from these positions, the reliable q interval from 0.13 to 35 nm^{-1}, where q is the magnitude of the scattering vector $q = 4\pi \sin(\theta)/\lambda$ and θ is half of the scattering angle, was reached. Measurements were performed in sealed capillaries of either boron glass or quartz with a diameter of 1.5 or 2 mm. Sample to detector distance was calibrated by means of a silver behenate or silicon standard. Data were azimuthally averaged and adjusted to an absolute scale using glassy carbon standard. The scattering curve of an empty capillary was subtracted from the scattering curves of samples.

Zeta potential measurements

The size, size distribution, and zeta potential of the vesicles were measured using a Malvern Zetasizer ultra instrument (Malvern Instruments, Malvern, UK) equipped with a 633 nm laser. Samples were diluted if needed in the same skin buffer as used before (pH 5.4) and filtered before measurements with a polyethersulfone 0.2 μm filter. Zeta potential for each sample was measured in triplicate (100 measuring points each), and the result is expressed as an average value ± standard deviation.

Permeation experiments

SC lipid models sandwiched between Teflon holders with an available diffusion area of 0.5 cm^2 were mounted in

Franz-type diffusion cells. The acceptor compartment was filled with PBS at pH 7.4 containing 50 mg/l gentamicin. The exact volume of buffer was individually measured for each cell and has been considered in flux calculations. Cells were equilibrated at 32°C, and the acceptor phase was stirred throughout the experiment. After 12 h equilibration at 32°C, transepidermal water loss (TEWL) and electrical impedance were measured. Then, 150 µl of either 5% theophylline (TH) or 2% indomethacin (IND) in 60% propylene glycol was applied to the membranes. Donor samples were saturated with model permeant to maintain the same thermodynamic activity throughout the experiment.

Samples of the acceptor phase (300 µl) were taken every 2 h over 10 h and were replaced by the same volume of freshly prepared PBS. During this period, a steady state was reached. The cumulative amounts of TH and IND that penetrated through the lipid membrane into the acceptor buffer were analyzed by HPLC, were corrected for the acceptor phase replacement and exact acceptor volume of the diffusion cells, and plotted as a function of time. Steady-state flux of TH or IND in $\mu g/(cm^2 \cdot h)$ was calculated as a slope of a linear regression function obtained by fitting the linear region of the plot in Microsoft Excel.

HPLC

Model permeants (TH and IND) in the acceptor phase samples were quantified by HPLC using a Shimadzu Prominence instrument (Kyoto, Japan) on a LiChroCART 250-4 column (LiChrospher 100 RP-18, 5 µm; Merck, Darmstadt, Germany). Mobile phases consisted of methanol/0.1 M NaH_2PO_4 in a 4:6 (v/v) ratio at 1.2 ml/min flow rate for TH and of acetonitrile/water/acetic acid in a 90:60:5 (v/v/v) ratio at 2 ml/min flow rate for IND. TH and IND were detected at 272 and 260 nm, respectively. Both methods were previously validated (32).

Water loss and electrical impedance

Water loss was measured in Franz diffusion cells after removing their upper parts using an AquaFlux AF200 instrument (Biox Systems Ltd, UK) at 61–62% relative air humidity and 23–24°C. The AquaFlux uses the condenser-chamber measurement method. The measured water loss value is defined as a steady-state flux of water diffusing through the membrane. The electrical impedance was measured using an LCR meter 4080 (Conrad Electronic, Hirschau, Germany) by immersing one electrode in the donor compartment filled with PBS for the purpose and the other one in the acceptor compartment of the cell (32–34). The data are presented as the mean ± standard deviation, and the number of replicates was n = 3–7. One-way analysis of variance with Tukey's post hoc test method was used for data comparison, using GraphPad Prism 9.2.0 (GraphPad SoftwarePro, San Diego, CA), and $P < 0.05$ was considered significant.

RESULTS

Zeta potential measurements on vesicles composed of Cer[NS]/FFA/Chol mixtures at varying concentrations of CholS

To study the influence of CholS on the SC lipid organization and structure, we compared three model mixtures mimicking the lipid composition of the SC that differ in their CholS contents: nCholS model with 0 mol% CholS; lCholS model with 5 mol% CholS, and hCholS model with 16.7 mol% CholS. Zeta potential measurements on sonicated vesicles composed of the three lipid mixtures showed decreasing surface potentials as the CholS content was increased. For the nCholS, a zeta potential of −9.1 ± 8.5 mV was determined. In the lCholS that contained 5 mol% CholS, the zeta potential dropped to −16.0 ± 1.8 mV, and for the hCholS containing 16.7 mol% CholS, the zeta potential was −42.4 ± 0.7 mV.

Investigation of the dynamics and phase state of the Cer[NS]/FFA/Chol/CholS mixture at various temperatures using ^2H NMR spectroscopy

Deuterated CholS-d_6 was synthesized from Chol-d_6 using HSO_3Cl in dry pyridine in a 79% yield. For each model, several samples with one ^2H-labeled lipid component each (either Cer[NS]-d_{47}, LA-d_{47}, Chol-d_6, or CholS-d_6) were prepared.

First, we analyzed the structure and dynamics of Cer[NS]-d_{47} containing a long C24:0 acyl chain. Stationary ^2H NMR spectra of this lipid in the mixture are shown in **Fig. 2**. Each column represents the ^2H NMR spectra of one SC model. Each row represents measurement at a given temperature between 25°C (bottom row) and 80°C (top row). Altogether, the figure provides an overview of the thermotropic phase behavior and the dynamics for Cer[NS]-d_{47} in the individual SC models. Numerical line shape simulations for all ^2H NMR spectra were performed and are shown as red lines in Fig. 2 allowing to quantify the respective phase proportions. These proportions are visualized as bar plots on the far right of Fig. 2 and assigned to specific lipid phases.

At 25°C, the ^2H NMR spectra of Cer[NS]-d_{47} in the mixture are dominated by one Pake doublet exhibiting a quadrupolar splitting of ~120 kHz indicating a rigid orthorhombic phase (10, 28, 30) for over 90% of the Cer[NS] in all three model mixtures. The terminal methyl groups undergo three-site rotations leading to partial averaging of the ^2H NMR lines (35). At physiological skin temperature of 32°C, we observe an important alteration of the ^2H NMR line shapes. In addition to the dominating crystalline phase, another highly ordered phase is observed that is simulated by a Pake doublet scaled with an order parameter (S) of ~0.7. Furthermore, about one-third of the spectral intensity is attributed to molecules in a fluid phase state ($S < 0.5$), whereas about two-thirds of the Cer[NS] in the mixture remain in a highly ordered orthorhombic phase state representing the basis to maintain the barrier function of the skin. Increasing the temperature to 50°C leads to further restructuring of the Cer[NS]. Now, only a minor fraction of the spectral intensity is attributed to the orthorhombic phase. In all three mixtures, the majority of the Cer[NS] component forms a relatively mobile phase, which is reminiscent of the liquid-ordered phase
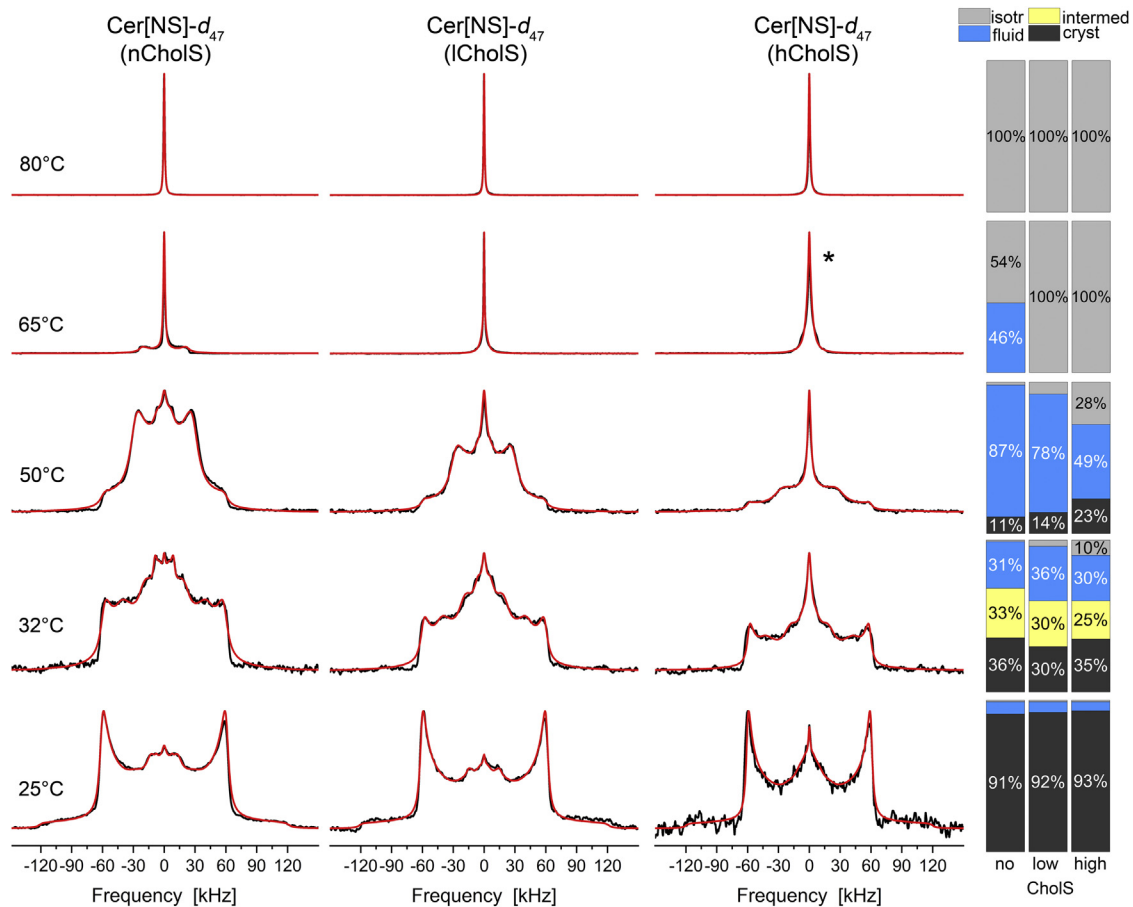
Fig. 2. ^{2}H NMR spectra and phase composition plots of Cer[NS]-d_{47} in the Cer[NS]/FFA mixture/Chol/CholS mixture (1/1/(1 − x)/x molar ratio) for different CholS-concentrations (x) at varying temperatures hydrated with 50 wt% buffer. The individual mixtures contain a mole fraction of CholS of the sterol components of x = 0 (nCholS model), x = 0.15 (lCholS model), and x = 0.5 (hCholS model), corresponding to total CholS contents of 0, 5, and 16.7 mol%, respectively. The bar plots on the right report the phase proportions derived from the numerical simulations of the ^{2}H NMR line shapes. The ^{2}H NMR spectra were acquired with a repetition time of up to 50 s. The red lines illustrate the best-fit numerical simulations. The spectrum labeled with * is simulated by two isotropic lines of different widths.

state as known from lipid raft mixtures (36–39). In this state, the lipid chains undergo axially symmetric reorientations in the membrane, while largely remaining in an all-*trans* state (36, 40). The resulting ^{2}H NMR spectra are characterized by a single quadrupolar splitting for the methylene segments with a width of ∼57.5 kHz (corresponding to a C-H order parameter of 0.46). The methyl groups are subject to three-site rotations, which scale their quadrupolar splitting by approximately one-third. In addition, smaller fractions of Cer[NS] still form an orthorhombic phase in all mixtures, whereas the hCholS model already shows 28% of the Cer[NS] molecules in an isotropic phase. Further increase in temperature to 65°C converts the majority of the Cer[NS] into an isotropic phase. For the nCholS model, 46% of the Cer[NS] is fluid and lamellar, whereas for the lCholS and hCholS models, we find the Cer[NS] largely in an isotropic state with some remaining order that accounts for a somewhat broader base of the ^{2}H NMR spectra. At 80°C, all Cer[NS] is found in an isotropic phase for all model mixtures.

Next, we studied the thermotropic phase behavior of LA-d_{47} as the most abundant FFA in human skin and compared it between the three models. The stationary ^{2}H NMR spectra of LA-d_{47} in the Cer[NS]/FFA mixture/Chol/CholS mixture at five different temperatures are shown in **Fig. 3**.

By and large, the ^{2}H NMR spectra of LA-d_{47} in the mixture are very similar to those of Cer[NS]-d_{47} with a perdeuterated C24:0 acyl chain as shown in Fig. 2. At 25°C, over 90% of the LA is organized in a highly ordered orthorhombic phase state for all mixtures observed. At physiological skin temperature (32°C), we observe similar partial fluidization. Again, about one-third of the LA is fluid, whereas two-thirds remain orthorhombic. However, the orthorhombic fraction of the spectral intensity is simulated with an order parameter of ∼1 and an approximately equal fraction with an order parameter of 0.7. Only in the hCholS model, about 13% of the LA is moving isotropically as also observed for Cer[NS]. Increasing the temperature to 50°C leads to a similar restructuring of the mixture
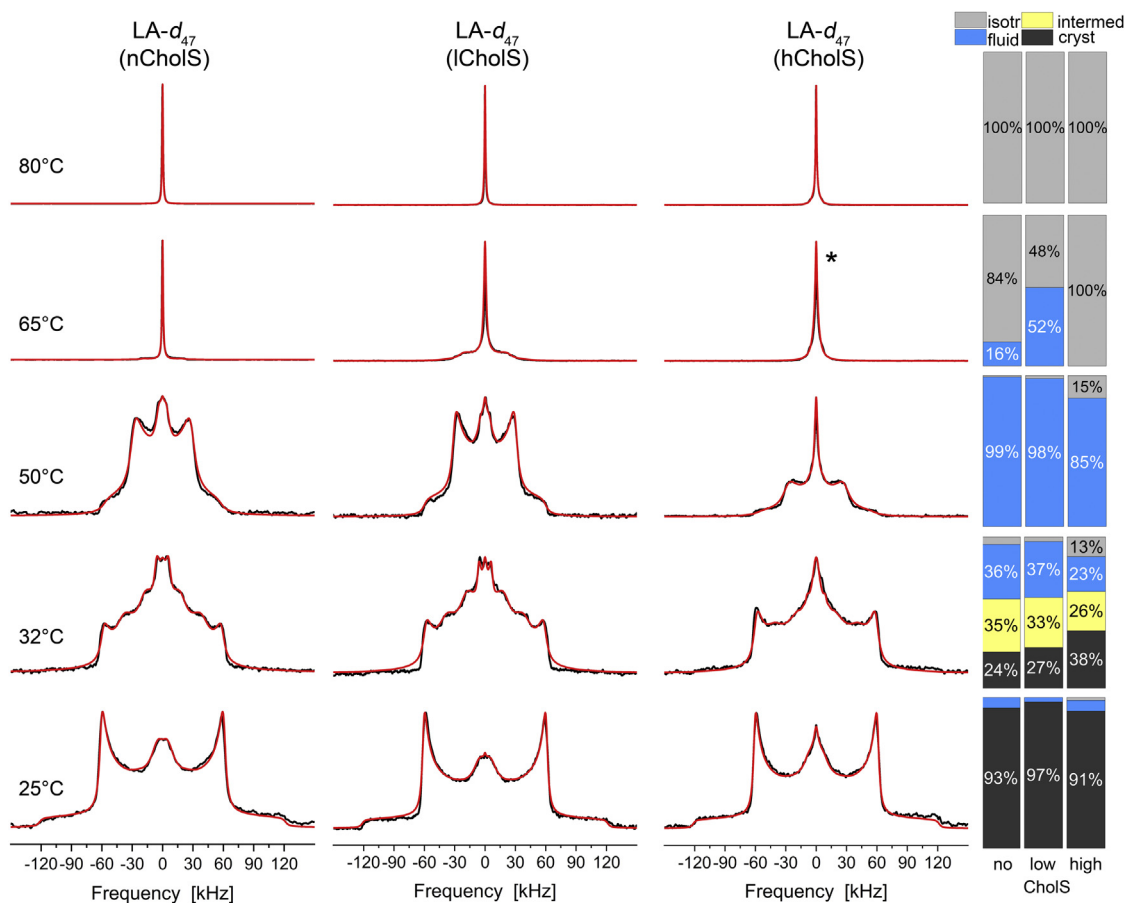
Fig. 3. ^{2}H NMR spectra and phase composition plots of LA-d_{47} in the Cer[NS]/FFA mixture/Chol/CholS mixture (1/1/(1 − x)/x molar ratio) for different CholS-concentrations (x) at varying temperatures hydrated with 50 wt% buffer. The individual mixtures contain a mole fraction of CholS of the sterol component of x = 0 (nCholS model), x = 0.15 (lCholS model), and x = 0.5 (hCholS model), corresponding to total CholS contents of 0, 5, and 16.7 mol%, respectively. The bar plots on the right report the phase proportions derived from the numerical simulations of the ^{2}H NMR line shapes. The ^{2}H NMR spectra were acquired with a repetition time of up to 50 s. The red lines illustrate the best-fit numerical simulations. The spectrum labeled with * is simulated by two isotropic phases.

as reported by Cer[NS]. However, there is no ortho-rhombic phase for LA anymore as opposed to what was observed for Cer[NS]. At 65°C, most of the LA converts into an isotropic phase, whereas for the lCholS model, about 52% remain fluid and lamellar. In the hCholS model, part of the LA is also not fully isotropic as indicated by a broad base of the isotropic line shape. At 80°C, LA is completely found in the isotropic phase in all model mixtures.

Next, we studied Chol-d_6 in the three model mixtures. The ^{2}H NMR spectra of Chol-d_6 in the Cer[NS]/FFA mixtures/Chol/CholS mixtures at five different temperatures are shown in **Fig. 4**.

Although increasing concentrations of CholS in the Cer[NS]/FFA mixture/Chol did not result in very prominent spectral changes for Cer[NS] and LA (compare **Figs. 2** and **3**), the phase state of Chol was highly influenced by the presence of increasing CholS concentrations (while simultaneously decreasing the Chol concentrations). At 25°C, the Chol in the CholS-free nCholS model is almost entirely (93%) in a

separated crystalline state. X-ray diffraction studies usually detect two populations of Chol, a population that is embedded in the lamellar structure and a population representing separated crystalline Chol (vide infra). For NMR, these crystalline phases are not distinguishable. However, very remarkably, the ^{2}H NMR spectra reveal that the crystalline Chol proportion decreases with increasing concentrations of CholS. In the absence of CholS, 93% of Chol are crystalline, whereas in the lCholS model that contains 5 mol% CholS, only 75% of the Chol is crystalline and 24% is fluid. In the hCholS model with 16.7% CholS, the crystalline proportion is further decreased to 43% and the fluid proportion increases to 54%. The fluid Chol that is found in the lCholS and hCholS models can be described as Chol in an upright orientation in the layers undergoing axially symmetric reorientations just as found in liquid-crystalline phospholipid bilayers (41, 42). At 32°C, this trend continues. The proportion of fluid Chol increases from 24% to 36% in the lCholS model and from 54% to 78% in the hCholS model.
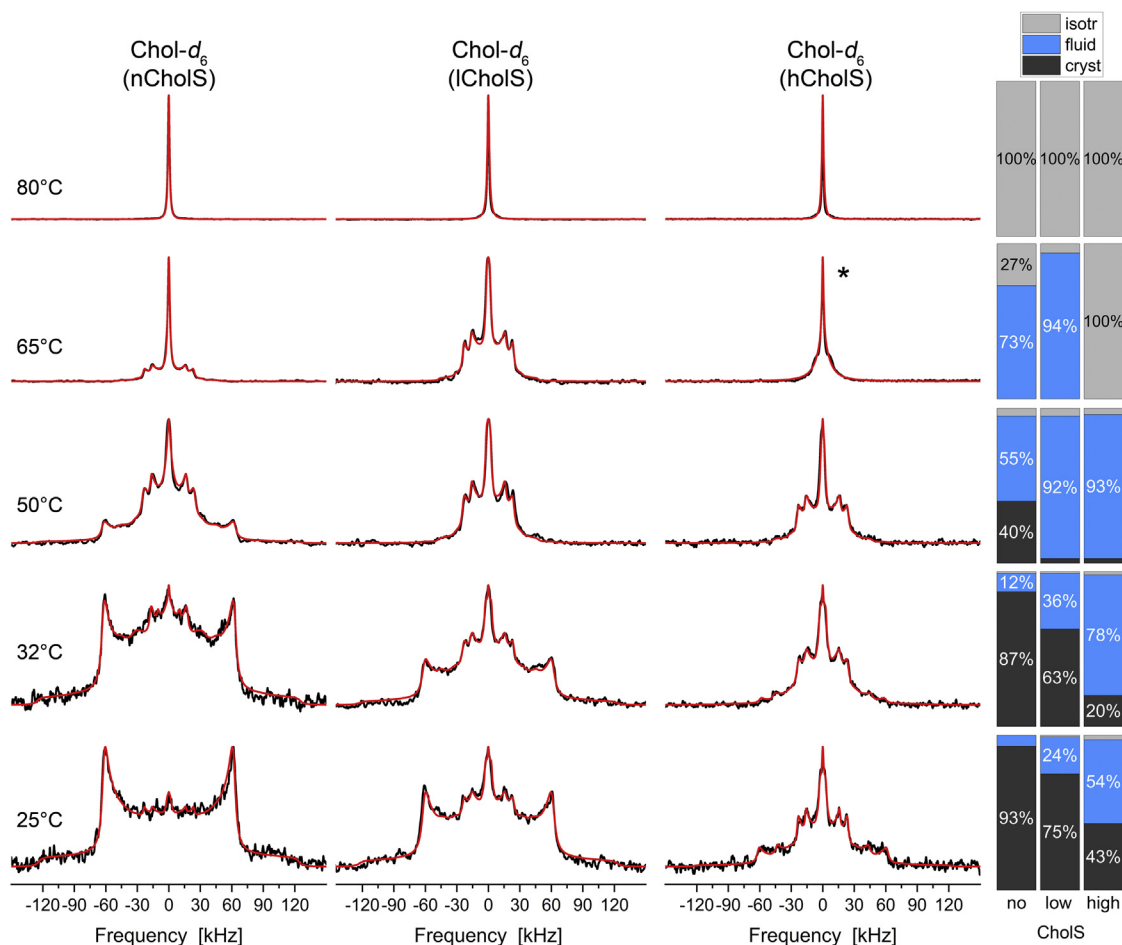
Fig. 4. ^{2}H NMR spectra and phase composition plots of Chol-d_6 in the Cer[NS]/FFA mixture/Chol/CholS mixture $(1/1/(1 − x)/x$ molar ratio) for different CholS concentrations (x) at varying temperatures hydrated with 50 wt% buffer. The individual mixtures contain a mole fraction of CholS of the sterol components of $x = 0$ (nCholS model), $x = 0.15$ (lCholS model), and $x = 0.5$ (hCholS model), corresponding to total CholS contents of 0, 5, and 16.7 mol%, respectively. The bar plots on the right report the phase proportions derived from the numerical simulations of the ^{2}H NMR line shapes. The ^{2}H NMR spectra were acquired with a repetition time of up to 50 s. The red lines illustrate the best-fit numerical simulations. The spectrum labeled with * is simulated by two isotropic phases.

Under these conditions, only 20% of the Chol are crystalline in the hCholS model, compared with 63% crystalline Chol in the lCholS model. At 50°C, Chol is still partially (40%) crystalline and partially (55%) fluid in the nCholS model, but in the lCholS and hCholS models, Chol-d_6 has almost entirely been converted to a predominantly fully fluid phase state (92 and 93%, respectively). Upon further heating to 65°C, Chol is showing a dominantly fluid behavior in the nCholS and lCholS mixtures. In the hCholS model, Chol is almost exclusively isotropic with some part undergoing slightly restricted motions as indicated by a broad base of the isotropic ^{2}H NMR line. At 80°C, Chol fully transitions into a completely isotropic phase as also observed for Cer[NS] and LA in the mixture.

Finally, we investigated the structure and dynamics of CholS in the lCholS and hCholS models. The ^{2}H NMR spectra of CholS-d_6 in the Cer[NS]/FFA mixture/Chol/ CholS mixture at five different temperatures are shown in **Fig. 5**. At 25°C and physiological skin temperature of

32°C, CholS forms a crystalline phase in the lCholS model (63%), whereas in the hCholS model, the fluid phase dominates the ^{2}H NMR spectrum (80%), and only a small fraction of 8% of the CholS is crystalline. Owing to the low spectral quality of the lCholS sample, which only contained 5 mol% CholS-d_6, the errors in the assignment of the respective phases are increased. At 50°C, CholS is predominantly fluid in both mixtures. Further temperature increase to 65°C converts all CholS into an isotropic phase in the hCholS model, whereas 86% of the CholS remains fluid in the lCholS model. At 80°C, all CholS is forming an isotropic phase in both models.

Taken together, the ^{2}H NMR studies show that increasing CholS/Chol ratios mainly fluidize the sterols of the lipid matrix, while having only marginal effects on the organization of Cer[NS] and LA.

X-ray SAXS and NWAXS measurements

The periodical structure of lipid models provided Bragg diffraction peaks superimposed over the
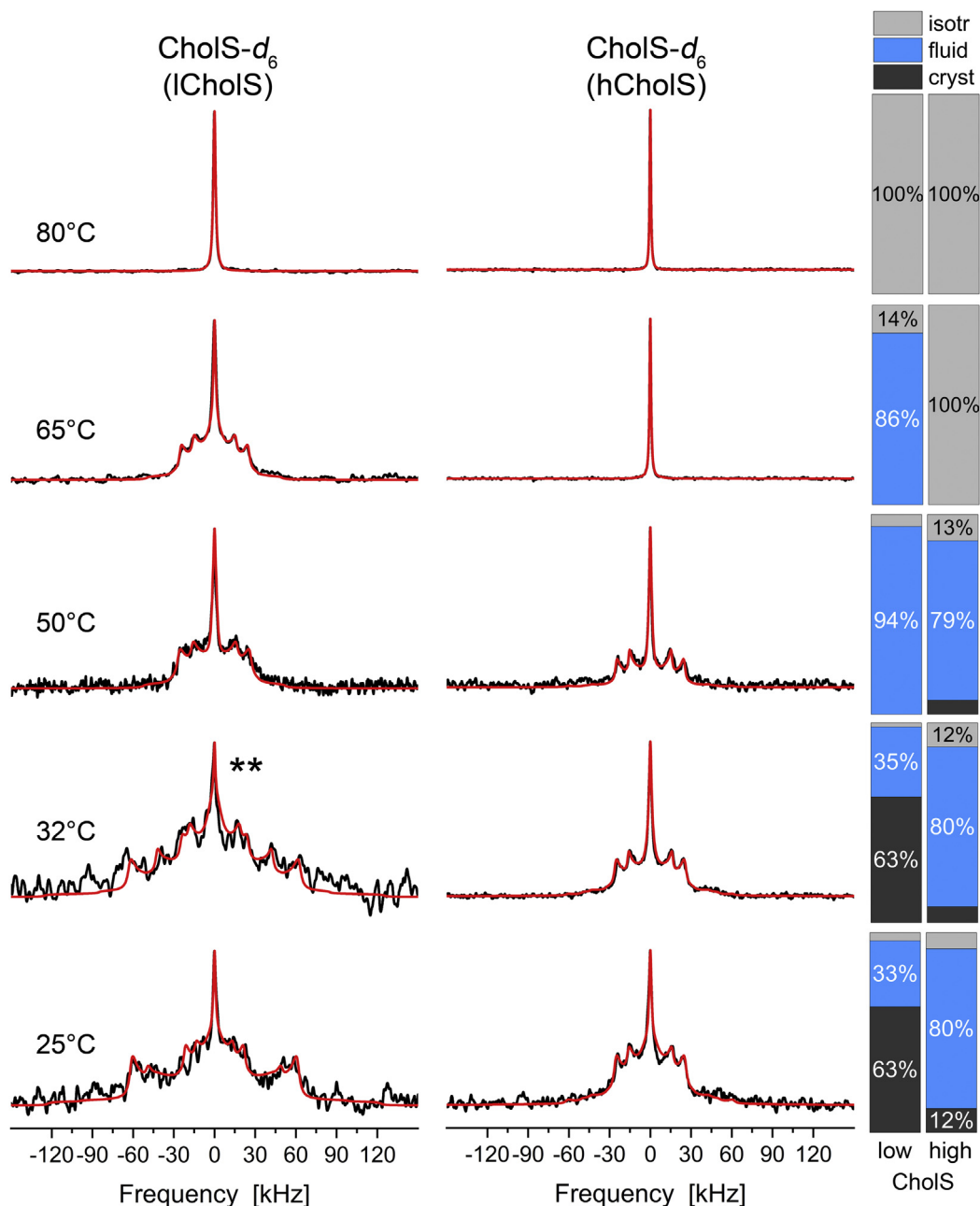
Fig. 5. ^{2}H NMR spectra and phase composition plots of CholS-d_6 in the Cer[NS]/FFA mixture/Chol/CholS mixture $(1/1/(1 − x)/x$ molar ratio) for different CholS concentrations (x) at varying temperatures hydrated with 50 wt% buffer. The individual mixtures contain a mole fraction of CholS of the sterol components of x = 0.15 (lCholS model) and x = 0.5 (hCholS model). The bar plots on the right report the phase proportions derived from the numerical simulations of the ^{2}H NMR line shapes. The ^{2}H NMR spectra were acquired with a repetition time of up to 50 s. The red lines illustrate the best-fit numerical simulations. The ^{2}H NMR spectrum labeled with ** is the sum of two beforehand processed measurements of the same mixture to improve the signal/noise ratio.

scattering/diffusive background in SAXS and NWAXS regions (**Fig. 6**). The samples for X-ray scattering were homogenized in the same way as samples for the ^{2}H NMR and measured in the presence of buffer at pH 5.4. In the SAXS region, all models showed a set of Bragg peaks with alternating relative intensities, which provided the repeat distance of 104.8–105.4 Å. The even orders were more intense than the odd orders, including the first-order peak, which was very weak and coincided with or was not

resolved from the exponentially decreasing scattering background. The measured structure is consistent with a medium lamellar phase (MLP) detected previously (20). The coexistence of MLP ($d \sim 105$ Å) with a phase having a half repeat distance (d $\sim$ 53 Å) cannot be excluded because they are commensurate phases. The patterns of nCholS and lCholS models also showed peaks of separated Chol at $q = 0.19$ Å^{-1} (convoluted with the third-order peak of MLP) and 0.37 Å^{-1}. Chol separation was more remarkable in the
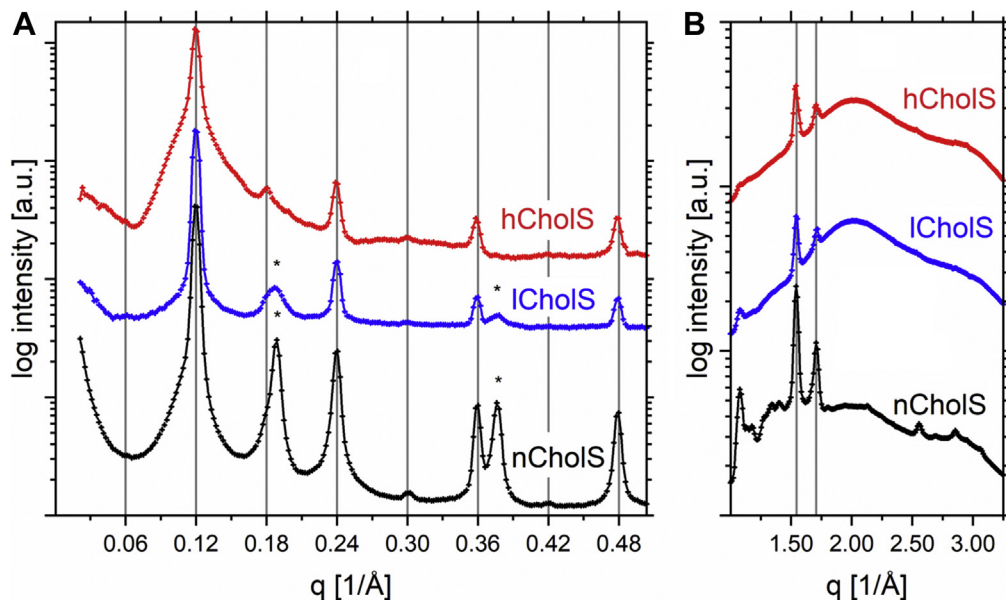
Fig. 6. The X-ray scattering patterns of the SAXS (A) and NWAXS (B) region. Gridlines in A predict the positions of Bragg peaks with the spacing of 105.3 Å; asterisks mark peaks of phase separated Chol. Grid lines B denote peaks of the orthorhombic phase at $q =$ 1.55 and 1.71 Å^{-1}.

sample with a higher content of Chol, that is, the nCholS model.

Two dominant peaks related to the chain packing subcell were detected in the NWAXS region of all samples at $q = 1.55$ and 1.71 Å^{-1}, corresponding to the repeat distances of the adjacent scattering planes of 4.1 and 3.7 Å. These peaks are typical for the tight orthorhombic crystal structure of polymethylene chains. Such tight arrangement is possible only in the chain domains without Chol molecules and is frequently found in crystalline lipids and *n*-alkanes (43). There were additional peaks in the NWAXS region of the nCholS sample (and partially in the patterns of the lCholS and hCholS models), located either at lower or higher q relative to the peaks of the orthorhombic subcell. Those at lower q originated most likely from the crystalline-separated Chol (44). It is not clear whether the peaks at higher q values came from separated Chol or orthorhombic subcell.

Permeability of model membranes

To check if the observed fluidization effect of CholS on the sterol components of the lipid matrix has functional consequences, we investigated the permeability of the model mixtures with varying CholS concentrations. These mixtures were investigated using four permeability markers, that is, TH and IND, as model permeants, water loss, and electrical impedance.

The membrane permeabilities to TH, a small molecule with balanced lipophilicity (molecular weight = 180.2 g/mol, logP ~0), as well as to the larger and more lipophilic IND (molecular weight = 357.8 g/mol, logP ~4.3), increased significantly with higher CholS proportion as

shown in **Fig. 7**. The flux of TH for lCholS model (0.41 ± 0.15 μg/[cm²·h]) was almost 3-fold higher than for the nCholS model (0.15 ± 0.09 μg/[cm²·h]). Further increase of the ratio of CholS to Chol resulted in an almost 2-fold higher TH flux in the hCholS model (0.74 ± 0.29 g/[cm²·h]) than the lCholS model indicating a significantly weaker barrier in the hCholS model compared with the normal skin model. The flux of IND shows the same trend, also rising with increasing CholS proportion, from 0.03 ± 0.01 μg/(cm²·h) in the nCholS model through 0.05 ± 0.02 μg/(cm²·h) in the lCholS model to 0.08 ± 0.02 μg/(cm²·h) in the hCholS model.

Water loss through the SC models was measured in the same manner and using the same instrumentation as TEWL, an established marker of the skin water barrier (45, 46). Upon increasing the ratio of CholS to Chol, water loss slightly increased from 17.51 ± 4.47 g/(m²·h) in the nCholS model to 19.32 ± 3.22 g/(m²·h) and 25.10 ± 5.74 g/(m²·h) in the lCholS and hCholS models, respectively.

Electrical impedance represents the membrane's resistance to alternating current. It is inversely proportional to the flux of charged particles, and in contrast to the other permeability markers, higher impedance values indicate lower permeability. The electrical impedance showed the same trend toward slightly higher permeability in the hCholS model (9.0 ± 4.7 kΩ × cm²) compared with the nCholS or lCholS models (114.0 ± 77.9 kΩ × cm² and 23.0 ± 6.5 kΩ × cm², respectively).

Taken together, our results indicate a rise in permeability to all investigated markers with an increasing CholS/Chol ratio. That corresponds well with our observations of higher fluidity of sterols in the presence of a higher CholS fraction.
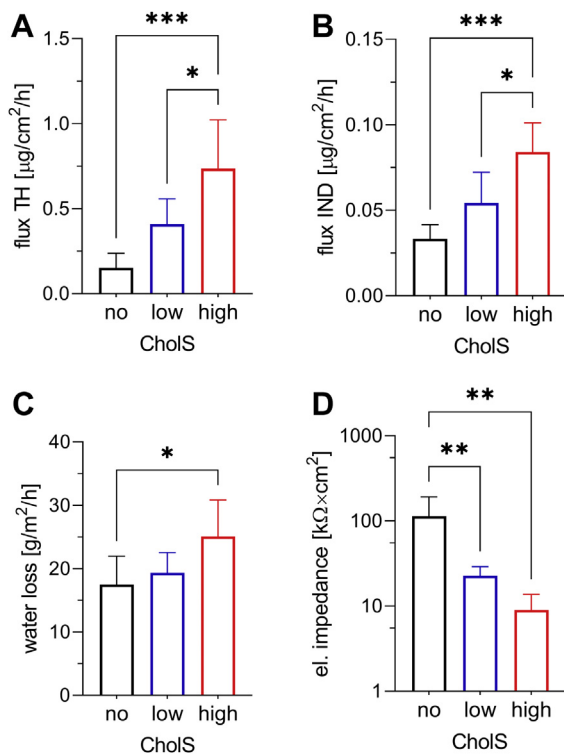
Fig. 7. Effects of CholS concentration (x) on the permeabilities of Cer[NS]/FFA mixture/Chol/CholS 1/1/(1 − x)/x molar ratio) model mixtures at 32°C. The permeability markers included flux of TH (A) or IND (B), water loss (C), and electrical impedance (D). Mixtures contained a total CholS mole fraction of 0% (nCholS model), 5% (lCholS model), or 16.7% (hCholS model); n = 3–7. Data are presented as the mean ± SD, and n is the number of replicates. Statistical significance against control: *$P < 0.05$; **$P < 0.01$; and ***$P < 0.001$.

DISCUSSION

The CholS/Chol cycle is an essential component of epidermal homeostasis and barrier development. The CholS concentration peaks in the first SC layers and decreases toward the outer SC layers along with the barrier maturation suggesting a role in regulating the barrier properties of the SC lipids. Indeed, patients suffering from XLI, who retain high CholS levels, display 40% increased TEWL [47, 48].

In this work, we investigated in detail the influence of the increasing substitution of Chol in SC model layers by CholS on the structure and dynamics of all lipid species of complex lipid mixtures. The sulfate group of CholS significantly alters the properties of the sterol molecule endowing it with several characteristic features. First, the sulfate group represents a much bulkier moiety compared with the hydroxyl group of Chol. With a volume of ~60 Å^3, it can potentially introduce a packing defect into the densely packed SC lipid layers compared with the much smaller hydroxyl group of Chol ($V \sim 20$ Å^3). Second, the sulfate group has a much higher hydrogen bonding capacity than Chol's hydroxyl group suggesting that this molecule may represent an important player in the lateral lipid

organization of the lipid phase of the SC. Third, the sulfate group has a high dipole moment of 4.7 D, which is likely engaged in additional electrostatic interactions with carbonyl or amide groups. Fourth, the sulfate group of CholS has a low pK_a [8], which suggests that it can be charged at a pH of 5.4 as present in the SC.

Indeed, for fully hydrated lipid vesicles prepared at this pH and with the same lipid composition as the SC model mixtures, we observed a decrease in the zeta potential of the vesicles with increasing CholS content, suggesting that the sulfate group is indeed negatively charged when exposed to an aqueous phase. It is known from multilamellar phospholipid preparations that the introduction of charged lipids leads to swelling of multilamellar preparations as electrostatic repulsion is not counterbalanced by attractive Van der Waals forces [49]. X-ray scattering experiments of our models showed that the lamellar repeat distance was not sensitive to the CholS/Chol ratios studied here (Fig. 6) in agreement with previous findings [50, 51]. The lack of water uptake of the CholS-containing SC layers provides a hint that CholS may not be equally distributed between the lipid layers of the SC models implying a heterogeneous CholS distribution in opposing lipid layers or leaflets. The repeat distance of approximately 105 Å is consistent with two asymmetric units as proposed previously on the basis of elegant X-ray diffraction data [20, 24]. In the nCholS and lCholS models, phase-separated crystalline Chol was detected, which disappeared in the hCholS model. This lack of separated Chol can be explained by decreased Chol content in that model and CholS-induced increase in the solubility of Chol in SC lipid mixtures [18, 19]. Therefore, when constructing a model of the SC unit cell in the presence of CholS, a homogeneous distribution of CholS in opposing layers has to be excluded.

In human SC, transmission electron microscopy images with RuO$_4$ staining typically have one to three trilamellar repeat units with a broad-narrow-broad sequence of electron-lucent bands with approximately 130 Å thickness in the SC [52–54], which most likely corresponds to the long periodicity phase described by X-ray diffraction, along with a 60 Å short periodicity phase [55, 56]. On the other hand, cryo-electron microscopy without staining revealed a repeat distance of 110 Å in mature SC layers [57] and 55–60 Å in immature SC layers [58]. Thus, the lamellar phases in the SC are still a matter of debate. Our models do not reproduce the long periodicity phase as we did not include the ω-O-acylceramides such as methyl-branched ceramide, which are essential for the 130 Å nm repeat unit. However, the propensity of these simplified models to form the 105 Å nm MLP phase with asymmetric lipid distribution may be an underlying principle of the SC lipid assembly in general and is likely further enhanced by the ω-O-acylceramides.

The ^{2}H NMR results show that Chol is the molecule of the SC mixture that is most strongly influenced by

the presence of CholS. Chol is classically known as a molecule that condenses phospholipid acyl chains (59–62). In contrast, in the very densely packed acyl chains of the SC lipid mixtures, sterols have to be considered as molecules that perturb the dense acyl chain packing and represent packing defects in the most densely packed chain regions rather than further increasing the packing density. CholS with its bulky sulfate group would introduce an even more significant packing defect than Chol. Thus, it is reasonable to assume that Chol and CholS are depleted in the FFA and Cer acyl chain region. This agrees with the finding that Chol is optimized to interact with lipids of 16 or 18 carbons (59). How could such an arrangement be visualized? Previous work indicates that the Cer molecules predominantly assume an extended conformation or a splayed conformation in the SC lipid films (9, 52, 57). One could imagine that the long FFAs along with the Cer's acyl chains are densely packed in all-*trans* conformation in one leaflet of the layers, and the sphingosine chains, short FFAs, Chol, and CholS in the other as proposed previously based on cryo-electron microscopy findings and infrared spectroscopy (57, 63). Such a scenario would require Chol and CholS to be asymmetrically distributed between the layers, which has indeed been found in a previous X-ray diffraction study (24). Thus, our interpretation of the increased mobility of the sterol component of the SC lipid models is based on that previous finding of an asymmetric lipid distribution within the SC lipid phase. On the basis of the ^{2}H NMR results alone, such an asymmetric lipid distribution cannot be concluded. Furthermore, our previous findings showed that the sphingosine chains of the Cer are found to be significantly more mobile than the acyl chains (9). To this end, the sphingosine chains of Cer molecules were deuterated, and the ^{2}H NMR experiments showed an astonishingly high mobility of these chains (9), whereas the Cer acyl chains remained highly rigid. These results can only be explained with an asymmetric lipid distribution in the SC lipid phase (24) as illustrated in a cartoon shown in **Fig. 8**. This likely is a consequence of the asymmetric distribution of the sterols and the specific colocalization with the sphingosine chains.

Such a model of the unit cell of the SC lipid phase would explain all experimental findings of the current study. When Chol is increasingly substituted by CholS, the solubility of Chol is also increased (18, 19) leading to more mobile sterols that associate with the more mobile sphingosine chains. Although the leaflet containing the Cer acyl chains and long FFAs remains densely packed, the barrier function of the other leaflet enriched in sterols, short FFAs, and the sphingosine chains is somewhat compromised leading to higher permeability. This means that CholS assumes the role of a modulator of the packing properties of the sphingosine-rich leaflet of the SC lipid phase. In the absence of CholS, only 7% of the Chol is fluid, but

the proportion of fluid Chol increases to 24% in the presence of 5 mol% CholS (lCholS model) and to 54% in the presence of 16.6 mol% CholS (hCholS model).

In stark contrast, neither the acyl chains of Cer[NS] nor the LA moieties of the SC lipid model are affected by the presence of either concentration of CholS (Figs. 2 and 3). This is very remarkable considering the decisive role Chol plays in acyl chain condensation (59–62) and the dynamic domain formation in phospholipid bilayers (37–39). As the increasing replacement of Chol by CholS in our preparations does not alter the dominance of the orthorhombic packing of acyl chains of Cer[NS] and LA, it must be concluded that both Chol and CholS are asymmetrically distributed in the lamellae and to a large extent separated from the long acyl chains in different leaflets of the lamellae (64, 65).

In the ^{2}H NMR spectra of Cer[NS] and LA at 32°C, we also detect a fraction of lipids with a quadrupolar splitting corresponding to an order parameter of 0.7. Order parameters represent a very useful tool to describe the orientation and/or motional amplitudes of lipids undergoing axially symmetric reorientations (66, 67). Lipids that undergo such motions exhibit an order parameter of ≤0.5. The fraction of lipids showing a chain order parameter of 0.7 is not undergoing axially symmetric reorientations. Rather, the order parameter of 0.7 can be interpreted as a tilting of the long axis of Cer[NS] or LA of ~63° relative to the membrane normal. This also supports the idea of asymmetric sterol distribution as the observed quadrupolar splittings of fluid Chol and CholS suggest a rather upright orientation of the sterols (41).

The logical question provoked by these results is if the alteration of the structure of the SC because of the presence of CholS has direct functional consequences on the permeability of the SC lipid models. Indeed, patients suffering from XLI have up to 40% increased TEWL (47, 48), but the direct effects of the increased CholS/Chol ratio on the water barrier cannot be inferred from these data as the changes induced by increased CholS in vivo are quite complex (the CholS actions involve, e.g., reduced serine protease activities, reduced HMG-CoA reductase activities, altered transglutaminase 1 activity, and increased expression of involucrin mRNA). To address this issue, we carried out permeation experiments employing four different permeation markers. Increased permeability of the model lipid film with higher CholS/Chol proportions was detected (Fig. 7), with the greatest differences between the nCholS and hCholS models. The increase in water permeability in our models indicates that the increased CholS/Chol ratio directly contributes to the altered water barrier also observed in XLI patients. In addition to the inside-out water barrier, we have shown that also the outside-in barrier is perturbed for both hydrophilic and lipophilic compounds, which is consistent with vascular response in XLI patients to topical hexyl nicotinate (48) and increased permeability
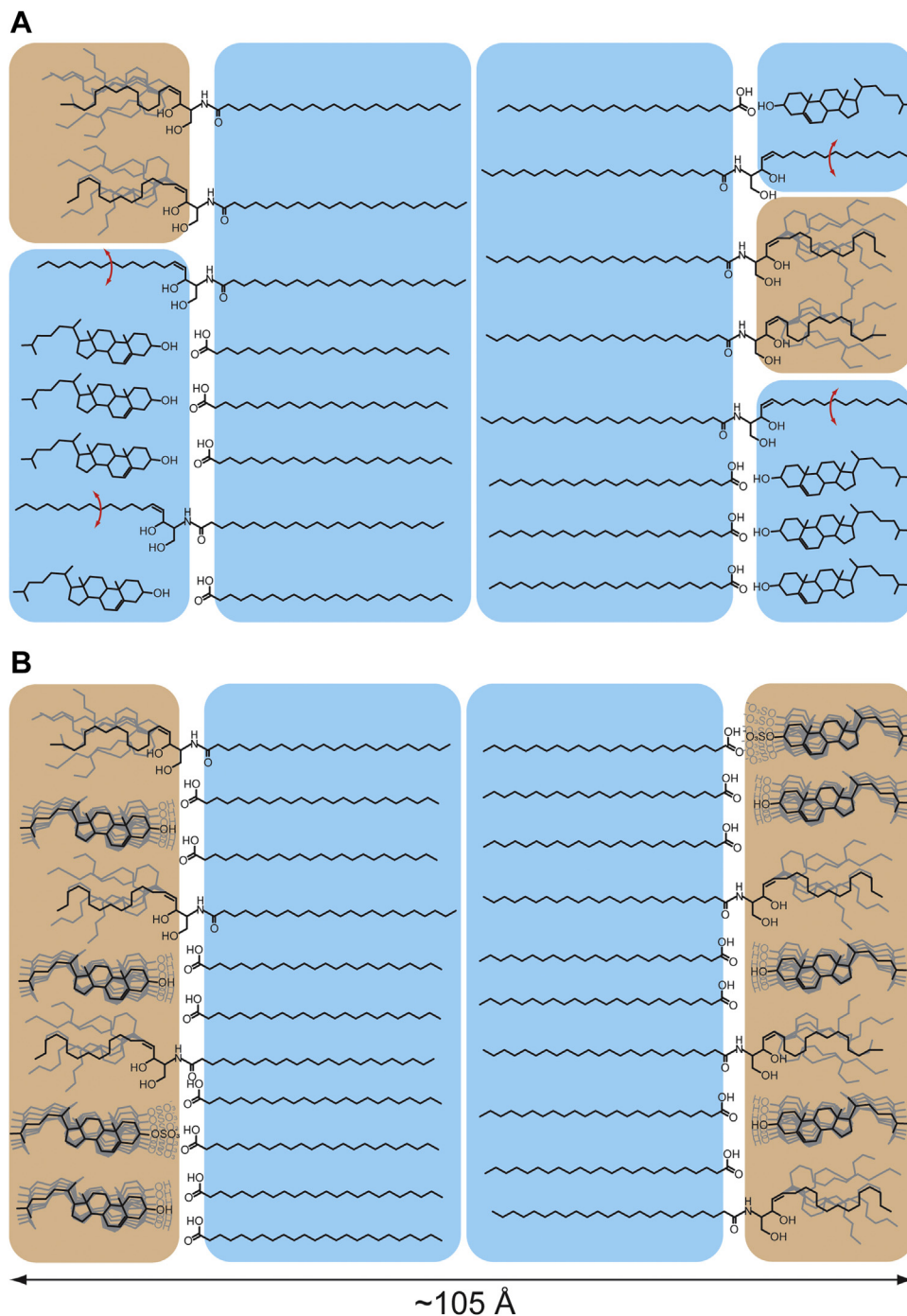
Fig. 8. Model of the distribution of the molecules in the SC lipid phase in the absence (A) and in the presence of CholS (B). In the absence of CholS (A), the Cer acyl chains, FFA, and Chol are essentially rigid in accordance with Engberg *et al.* (9). The sphingosine chains are partly highly mobile or in all-*trans* conformation undergoing two-site hopping (indicated by red arrows). Chol is asymmetrically dis tributed in one leaflet and largely segregated from the sphingosine chains. Addition of CholS (B) fluidizes the sterol component of the mixture, but the acyl chains of the FFA and Cer remain highly rigid. The rigid assembly of the acyl chains is indicated by blue color and the mobile Chol, CholS, and sphingosine region by orange areas.

to benzoic acid of a previous lipid model with a 1:3 CholS/Chol ratio compared with a model without CholS (68).

The decreased lipid rigidity in the sterol-rich leaflet and increased permeability in our simplified models are broadly consistent with the increased skin permeability in diseased phenotypes. Although the impaired

CholS desulfation alters many factors in epidermal homeostasis (7), our findings show that an increased CholS/Chol ratio directly contributes to the abrogated barrier by rendering the sterol fraction of the lipid fluid and permeable to compounds of various physicochemical properties. In addition, the sterol fluidity decrease upon exchange of CholS for Chol is likely

relevant to the lipid remodeling during SC maturation. The fluidity induced by high CholS may be important for the SC lipids to attain their complex architecture, for example, for the Cer chain flip suggested upon Cer release from its precursors (58, 65). The CholS desulfation to Chol and rigidification of the lipid mixture then likely contribute to a competent permeability barrier of healthy human skin.

Finally, it should be mentioned that the biophysical models though providing detailed structural and dynamical data with atomic resolution represent a distinct simplification of the very complex biological diversity of lipid species relevant for the SC lipid phase. Nevertheless, such models have advanced our understanding of the highly complex biological situation, and physiological studies may further confirm the fluidizing effect of CholS on the sterol component of the SC lipid phase.

CONCLUSION

The findings of the current study are summarized in the cartoon shown in Fig. 8 and extend our understanding of the SC lipid barrier. The presence of a low but physiological amount of CholS induces higher sterol fluidity than the SC lipid model without CholS. A higher CholS/Chol ratio induces much higher sterol fluidity leading to higher permeabilities of the lipid layers, despite the long acyl chains of FFAs and Cers staying rigid. Our data confirm an asymmetric distribution of sterols and acyl chains in the SC lipid lamellae and that selective fluidization of the sterol-rich leaflet of the lamella may significantly alter the overall barrier function of such lipids. Putatively, such selective sterol fluidization might serve as a useful target for enhancing transdermal drug delivery, for example, with CholS as a pharmaceutical lead for future penetration enhancers, provided its signaling properties are markedly attenuated.

Author contributions
F. F., K. V., and D. H. methodology; F. F., O. E., P. P., P. J., M. S., and A. K. formal analysis; L. O., F. F., O. E., P. P., P. J., M. S., and A. K. investigation; F. F., K. V., and D. H. writing–original draft.

Author ORCIDs
Oskar Engberg ⓘ https://orcid.org/0000-0002-0284-5504
Lukáš Opálka ⓘ https://orcid.org/0000-0003-1379-1406
Pavla Jančálková ⓘ https://orcid.org/0000-0001-8990-5970
Petra Pullmannová ⓘ https://orcid.org/0000-0001-5801-5094
Andrej Kováčik ⓘ https://orcid.org/0000-0002-5597-3155
Kateřina Vávrová ⓘ https://orcid.org/0000-0002-8502-4372
Daniel Huster ⓘ https://orcid.org/0000-0002-3273-0943

Conflict of interest
The authors declare that they have no conflicts of interest with the contents of this article.

Abbreviations
Cer, ceramide; Cer[NS], N-lignoceroyl-D-erythro-sphingosine; Cer[NS]-d_{47}, N-lignoceroyl-D-erythro-sphingosine-d_{47}; Chol, cholesterol; Chol-d_6, cholesterol (2H-2,2,3,4,4,6); CholS, cholesterol sulfate; CholS-d_6, cholesterol sulfate-d_6; FFA, free fatty acid; hCholS, high CholS; IND, indomethacin; LA, lignoceric acid; LA-d_{47}, lignoceric acid-d_{47}; lCholS, low CholS; MLP, medium lamellar phase; nCholS, no CholS; NWAXS, near wide-angle X-ray scattering; SAXS, small-angle X-ray scattering; SC, stratum corneum; TEWL, transepidermal water loss; TH, theophylline; XLI, X-linked ichthyosis.

REFERENCES

1. Bouwstra, J. A., and Ponec, M. (2006) The skin barrier in healthy and diseased state. *Biochim. Biophys. Acta.* **1758**, 2080–2095
2. Feingold, K. R., and Elias, P. M. (2014) Role of lipids in the formation and maintenance of the cutaneous permeability barrier. *Biochim. Biophys. Acta.* **1841**, 280–294
3. van Smeden, J., Janssens, M., Gooris, G. S., and Bouwstra, J. A. (2014) The important role of stratum corneum lipids for the cutaneous barrier function. *Biochim. Biophys. Acta.* **1841**, 295–313
4. van Smeden, J., and Bouwstra, J. A. (2016) Stratum corneum lipids: their role for the skin barrier function in healthy subjects and atopic dermatitis patients. *Curr. Probl. Dermatol.* **49**, 8–26
5. Elias, P. M., Crumrine, D., Rassner, U., Hachem, J. P., Menon, G. K., Man, W., Choy, M. H., Leypoldt, L., Feingold, K. R., and Williams, M. L. (2004) Basis for abnormal desquamation and permeability barrier dysfunction in RXLI. *J. Invest. Dermatol.* **122**, 314–319
6. Elias, P. M., Williams, M. L., Maloney, M. E., Bonifas, J. A., Brown, B. E., Grayson, S., and Epstein, E. H., Jr. (1984) Stratum corneum lipids in disorders of cornification. Steroid sulfatase and cholesterol sulfate in normal desquamation and the pathogenesis of recessive X-linked ichthyosis. *J. Clin. Invest.* **74**, 1414–1421
7. Elias, P. M., Williams, M. L., Choi, E. H., and Feingold, K. R. (2014) Role of cholesterol sulfate in epidermal structure and function: lessons from X-linked ichthyosis. *Biochim. Biophys. Acta.* **1841**, 353–361
8. Bleau, G., Roberts, K. D., and Chapdelaine, A. (1974) Cholesterol sulfate. I. Occurrence and possible biological functions as an

amphipathic lipid in the membrane of the human erythrocyte. *Biochim. Biophys. Acta.* **352**, 1–9

9. Engberg, O., Kovacik, A., Pullmannová, P., Juhaščik, M., Opálka, L., H, D., and Vávrová, K. (2020) The sphingosine and acyl chains of ceramide [NS] show very different structure and dynamics challenging our understanding of the skin barrier. *Angew. Chem. Int. Ed. Engl.* **59**, 17383–17387

10. Paz Ramos, A., Gooris, G., Bouwstra, J., and Lafleur, M. (2018) Evidence of hydrocarbon nanodrops in highly ordered stratum corneum model membranes. *J. Lipid Res.* **59**, 137–143

11. Wang, E., and Klauda, J. B. (2019) Molecular structure of the long periodicity phase in the stratum corneum. *J. Am. Chem. Soc.* **141**, 16930–16943

12. Bouwstra, J. A., Gooris, G. S., Dubbelaar, F. E., and Ponec, M. (2001) Phase behavior of lipid mixtures based on human ceramides: coexistence of crystalline and liquid phases. *J. Lipid Res.* **42**, 1759–1770

13. Wiener, M. C., and White, S. H. (1992) Structure of a fluid dioleoylphosphatidylcholine bilayer determined by joint refinement of x-ray and neutron diffraction data III. Complete structure. *Biophys. J.* **61**, 434–447

14. Huster, D., Arnold, K., and Gawrisch, K. (1999) Investigation of lipid organization in biological membranes by two-dimensional nuclear overhauser enhancement spectroscopy. *J. Phys. Chem. B.* **103**, 243–251

15. Mojumdar, E. H., Gooris, G. S., Barlow, D. J., Lawrence, M. J., Deme, B., and Bouwstra, J. A. (2015) Skin lipids: localization of ceramide and fatty acid in the unit cell of the long periodicity phase. *Biophys. J.* **108**, 2670–2679

16. Israelachvili, J. N. (1992) Intermolecular and Surface Forces. Academic Press, London

17. Huster, D., Jin, A. J., Arnold, K., and Gawrisch, K. (1997) Water permeability of polyunsaturated lipid membranes measured by ^{17}O NMR. *Biophys. J.* **73**, 855–864

18. Bouwstra, J. A., Gooris, G. S., Dubbelaar, F. E., and Ponec, M. (1999) Cholesterol sulfate and calcium affect stratum corneum lipid organization over a wide temperature range. *J. Lipid Res.* **40**, 2303–2312

19. Bouwstra, J. A., Gooris, G. S., Dubbelaar, F. E., Weerheim, A. M., and Ponec, M. (1998) pH, cholesterol sulfate, and fatty acids affect the stratum corneum lipid organization. *J. Investig. Dermatol. Symp. Proc.* **3**, 69–74

20. Pullmannová, P., Ermakova, E., Kovacik, A., Opalka, L., Maixner, J., Zbytovska, J., Kucerka, N., and Vavrova, K. (2019) Long and very long lamellar phases in model stratum corneum lipid membranes. *J. Lipid Res.* **60**, 963–971

21. Bastiat, G., and Lafleur, M. (2007) Phase behavior of palmitic acid/cholesterol/cholesterol sulfate mixtures and properties of the derived liposomes. *J. Phys. Chem. B.* **111**, 10929–10937

22. Groen, D., Gooris, G. S., and Bouwstra, J. A. (2010) Model membranes prepared with ceramide EOS, cholesterol and free fatty acids form a unique lamellar phase. *Langmuir.* **26**, 4168–4175

23. Williams, M. L., and Elias, P. M. (1981) Stratum corneum lipids in disorders of cornification: increased cholesterol sulfate content of stratum corneum in recessive x-linked ichthyosis. *J. Clin. Invest.* **68**, 1404–1410

24. McIntosh, T. J. (2003) Organization of skin stratum corneum extracellular lamellae: diffraction evidence for asymmetric distribution of cholesterol. *Biophys. J.* **85**, 1675–1681

25. Kovacik, A., Vogel, A., Adler, J., Pullmannova, P., Vavrova, K., and Huster, D. (2018) Probing the role of ceramide hydroxylation in skin barrier lipid models by 2H solid-state NMR spectroscopy and X-ray powder diffraction. *Biochim. Biophys. Acta.* **1860**, 1162–1170

26. van Smeden, J., Boiten, W. A., Hankemeier, T., Rissmann, R., Bouwstra, J. A., and Vreeken, R. J. (2014) Combined LC/MS-platform for analysis of all major stratum corneum lipids, and the profiling of skin substitutes. *Biochim. Biophys. Acta.* **1841**, 70–79

27. Davis, J. H., Jeffrey, K. R., Bloom, M., Valic, M. I., and Higgs, T. P. (1976) Quadrupolar echo deuteron magnetic resonance spectroscopy in ordered hydrocarbon chains. *Chem. Phys. Lett.* **42**, 390–394

28. Brief, E., Kwak, S., Cheng, J. T., Kitson, N., Thewalt, J., and Lafleur, M. (2009) Phase behavior of an equimolar mixture of N-palmitoyl-D-erythro-sphingosine, cholesterol, and palmitic acid, a mixture with optimized hydrophobic matching. *Langmuir.* **25**, 7523–7532

29. Huster, D., Arnold, K., and Gawrisch, K. (1998) Influence of docosahexaenoic acid and cholesterol on lateral lipid organization in phospholipid membranes. *Biochemistry.* **37**, 17299–17308

30. Stahlberg, S., Skolova, B., Madhu, P. K., Vogel, A., Vavrova, K., and Huster, D. (2015) Probing the role of the ceramide acyl chain length and sphingosine unsaturation in model skin barrier lipid mixtures by 2H solid-state NMR spectroscopy. *Langmuir.* **31**, 4906–4915

31. Kitson, N., Thewalt, J., Lafleur, M., and Bloom, M. (1994) A model membrane approach to the epidermal permeability barrier. *Biochemistry.* **33**, 6707–6715

32. Skolova, B., Kovacik, A., Tesar, O., Opalka, L., and Vavrova, K. (2017) Phytosphingosine, sphingosine and dihydrosphingosine ceramides in model skin lipid membranes: permeability and biophysics. *Biochim. Biophys. Acta.* **1859**, 824–834

33. Pullmannova, P., Pavlikova, L., Kovacik, A., Sochorova, M., Skolova, B., Slepicka, P., Maixner, J., Zbytovska, J., and Vavrova, K. (2017) Permeability and microstructure of model stratum corneum lipid membranes containing ceramides with long (C16) and very long (C24) acyl chains. *Biophys. Chem.* **224**, 20–31

34. Sochorova, M., Audrlicka, P., Cervena, M., Kovacik, A., Kopecna, M., Opalka, L., Pullmannova, P., and Vavrova, K. (2019) Permeability and microstructure of cholesterol-depleted skin lipid membranes and human stratum corneum. *J. Colloid Interf. Sci.* **535**, 227–238

35. Beshah, K., Olejniczak, E. T., and Griffin, R. G. (1987) Deuterium NMR study of methyl group dynamics in *L*-alanine. *J. Chem. Phys.* **86**, 4730–4736

36. Polozov, I. V., and Gawrisch, K. (2006) Characterization of the liquid-ordered state by proton MAS NMR. *Biophys. J.* **90**, 2051–2061

37. Bunge, A., Müller, P., Stöckl, M., Herrmann, A., and Huster, D. (2008) Characterization of the ternary mixture of sphingomyelin, POPC, and cholesterol: support for an inhomogeneous lipid distribution at high temperatures. *Biophys. J.* **94**, 2680–2690

38. Bartels, T., Lankalapalli, R. S., Bittman, R., Beyer, K., and Brown, M. F. (2008) Raftlike mixtures of sphingomyelin and cholesterol investigated by solid-state ^{2}H NMR spectroscopy. *J. Am. Chem. Soc.* **130**, 14521–14532

39. Veatch, S. L., Soubias, O., Keller, S. L., and Gawrisch, K. (2007) Critical fluctuations in domain-forming lipid mixtures. *Proc. Natl. Acad. Sci. U. S. A.* **104**, 17650–17655

40. Hutchison, J. M., Shih, K. C., Scheidt, H. A., Fantin, S. M., Parson, K. F., Pantelopulos, G. A., Harrington, H. R., Mittendorf, K. F., Qian, S., Stein, R. A., Collier, S. E., Chambers, M. G., Katsaras, J., Voehler, M. W., Ruotolo, B. T., *et al.* (2020) Bicelles rich in both sphingolipids and cholesterol and their use in studies of membrane proteins. *J. Am. Chem. Soc.* **142**, 12715–12729

41. Dufourc, E. J., Parish, E. J., Chitrakorn, S., and Smith, C. P. (1984) Structural and dynamical details of cholesterol-lipid interaction as revealed by deuterium NMR. *Biochemistry.* **23**, 6062–6071

42. Taylor, M. G., Akiyama, T., and Smith, I. C. P. (1981) The molecular dynamics of cholesterol in bilayer membranes: a deuterium NMR study. *Chem. Phys. Lipids.* **29**, 327–339

43. Marsh, D. (2012) Lateral order in gel, subgel and crystalline phases of lipid membranes: wide-angle X-ray scattering. *Chem. Phys. Lipids.* **165**, 59–76

44. Bouwstra, J. A., Honeywell-Nguyen, P. L., Gooris, G. S., and Ponec, M. (2003) Structure of the skin barrier and its modulation by vesicular formulations. *Prog. Lipid Res.* **42**, 1–36

45. Grubauer, G., Elias, P. M., and Feingold, K. R. (1989) Transepidermal water loss: the signal for recovery of barrier structure and function. *J. Lipid Res.* **30**, 323–333

46. Netzlaff, F., Kostka, K. H., Lehr, C. M., and Schaefer, U. F. (2006) TEWL measurements as a routine method for evaluating the integrity of epidermis sheets in static Franz type diffusion cells in vitro. Limitations shown by transport data testing. *Eur. J. Pharm. Biopharm.* **63**, 44–50

47. Zettersten, E., Man, M. Q., Sato, J., Denda, M., Farrell, A., Ghadially, R., Williams, M. L., Feingold, K. R., and Elias, P. M. (1998) Recessive x-linked ichthyosis: role of cholesterol-sulfate accumulation in the barrier abnormality. *J. Invest. Dermatol.* **111**, 784–790

48. Lavrijsen, A. P., Oestmann, E., Hermans, J., Bodde, H. E., Vermeer, B. J., and Ponec, M. (1993) Barrier function parameters in various keratinization disorders: transepidermal water loss and vascular response to hexyl nicotinate. *Br. J. Dermatol.* **129**, 547–553

ASBMB

49. Rand, R. P., and Parsegian, V. A. (1989) Hydration forces between phospholipid bilayers. *Biochim. Biophys. Acta.* **988**, 351–376
50. Bouwstra, J. A., Gooris, G. S., van der Spek, J. A., Lavrijsen, S., and Bras, W. (1994) The lipid and protein structure of mouse stratum corneum: a wide and small angle diffraction study. *Biochim. Biophys. Acta.* **1212**, 183–192
51. McIntosh, T. J., Stewart, M. E., and Downing, D. T. (1996) X-ray diffraction analysis of isolated skin lipids: reconstitution of intercellular lipid domains. *Biochemistry.* **35**, 3649–3653
52. Swartzendruber, D. C., Wertz, P. W., Kitko, D. J., Madison, K. C., and Downing, D. T. (1989) Molecular models of the intercellular lipid lamellae in mammalian stratum corneum. *J. Invest. Dermatol.* **92**, 251–257
53. Bouwstra, J. A., Gooris, G. S., van der Spek, J. A., and Bras, W. (1991) Structural investigations of human stratum corneum by small-angle X-ray scattering. *J. Invest. Dermatol.* **97**, 1005–1012
54. Hill, J. R., and Wertz, P. W. (2003) Molecular models of the intercellular lipid lamellae from epidermal stratum corneum. *Biochim. Biophys. Acta.* **1616**, 121–126
55. Bouwstra, J. A., Gooris, G. S., Salomons-d Vries, M. A., van der Spek, J. A., and Bras, W. (1992) Structure of human stratum corneum as a function of temperature and hydration: a wide-angle X-ray diffraction. *Int. J. Pharm.* **84**, 205–216
56. Hou, S. Y., Mitra, A. K., White, S. H., Menon, G. K., Ghadially, R., and Elias, P. M. (1991) Membrane structures in normal and essential fatty acid-deficient stratum corneum: characterization by ruthenium tetroxide staining and x-ray diffraction. *J. Invest. Dermatol.* **96**, 215–223
57. Iwai, I., Han, H., den, H. L., Svensson, S., Ofverstedt, L. G., Anwar, J., Brewer, J., Bloksgaard, M., Laloeuf, A., Nosek, D., Masich, S., Bagatolli, L. A., Skoglund, U., and Norlen, L. (2012) The human skin barrier is organized as stacked bilayers of fully extended ceramides with cholesterol molecules associated with the ceramide sphingoid moiety. *J. Invest. Dermatol.* **132**, 2215–2225
58. Narangifard, A., Wennberg, C. L., den Hollander, L., Iwai, I., Han, H., Lundborg, M., Masich, S., Lindahl, E., Daneholt, B., and Norlen, L. (2021) Molecular reorganization during the formation of the human skin barrier studied in situ. *J. Invest. Dermatol.* **141**, 1243–1253.e6
59. Scheidt, H. A., Meyer, T., Nikolaus, J., Baek, D. J., Haralampiev, I., Thomas, L., Bittman, R., Herrmann, A., Müller, P., and Huster, D. (2013) Cholesterol's aliphatic side chain structure modulates membrane properties. *Angew. Chem. Int. Ed. Engl.* **52**, 12848–12851
60. Almeida, P. F., Pokorny, A., and Hinderliter, A. (2005) Thermodynamics of membrane domains. *Biochim. Biophys. Acta.* **1720**, 1–13
61. Davies, M. A., Schuster, H. F., Brauner, J. W., and Mendelsohn, R. (1990) Effects of cholesterol on conformational disorder in dipalmitoylphosphatidylcholine bilayers. A quantitative IR study on the depth dependence. *Biochemistry.* **29**, 4368–4373
62. Huang, C. H. (1977) A structural model for the cholesterol-phosphatidylcholine complexes in bilayer membranes. *Lipids.* **12**, 348–356
63. Skolova, B., Hudska, K., Pullmannova, P., Kovacik, A., Palat, K., Roh, J., Fleddermann, J., Hrabalek, A., Estrela-Lopis, I., and Vavrova, K. (2014) Different phase behavior and packing of ceramides with long (Cl6) and very long (C24) acyls in model membranes: infrared spectroscopy using deuterated lipids. *J. Phys. Chem. B.* **118**, 10460–10470
64. Beddoes, C. M., Gooris, G. S., and Bouwstra, J. A. (2018) Preferential arrangement of lipids in the long-periodicity phase of a stratum corneum matrix model. *J. Lipid Res.* **59**, 2329–2338
65. Novackova, A., Sagrafena, I., Pullmannova, P., Paraskevopoulos, G., Dwivedi, A., Mazumder, A., Ruzickova, K., Slepicka, P., Zbytovska, J., and Vavrova, K. (2021) Acidic pH is required for the multilamellar assembly of skin barrier lipids in vitro. *J. Invest. Dermatol.* **141**, 1915–1921.e4
66. Davis, J. H. (1979) Deuterium magnetic resonance study of the gel and liquid crystalline phases of dipalmitoyl phosphocholine. *Biophys. J.* **27**, 339–358
67. Seelig, J. (1977) Deuterium magnetic resonance: theory and application to lipid membranes. *Q. Rev. Biophys.* **10**, 353–418
68. Groen, D., Poole, D. S., Gooris, G. S., and Bouwstra, J. A. (2011) Investigating the barrier function of skin lipid models with varying compositions. *Eur. J. Pharm. Biopharm.* **79**, 334–342